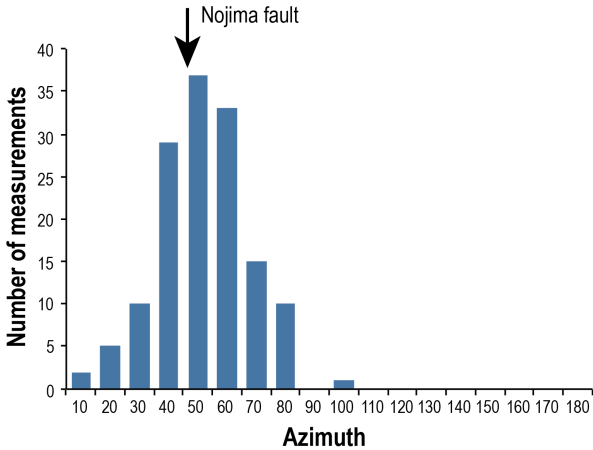
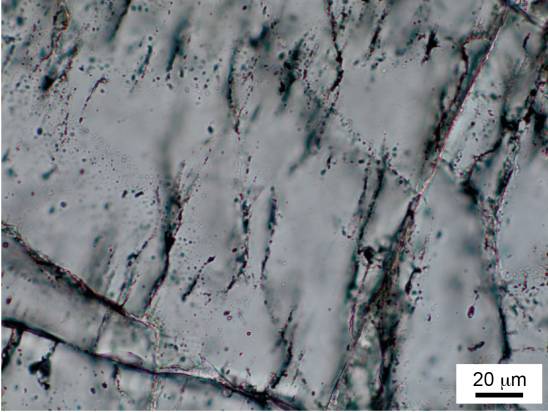


# Supplementary material

a - Alignments of tiny fluid inclusions



b - Kink-bands in biotites

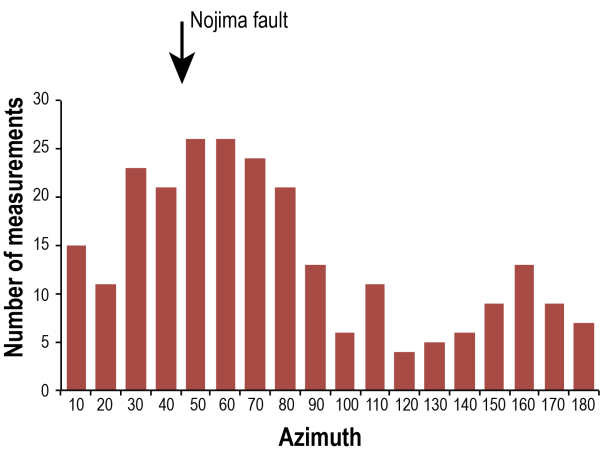
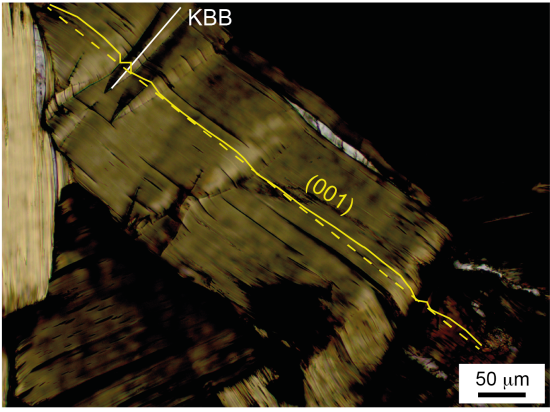


Figure S1 – Microphotographs and orientation histograms of (a) alignments of tiny fluid inclusions and (b) kinks in biotites in the NOJ220 sample.

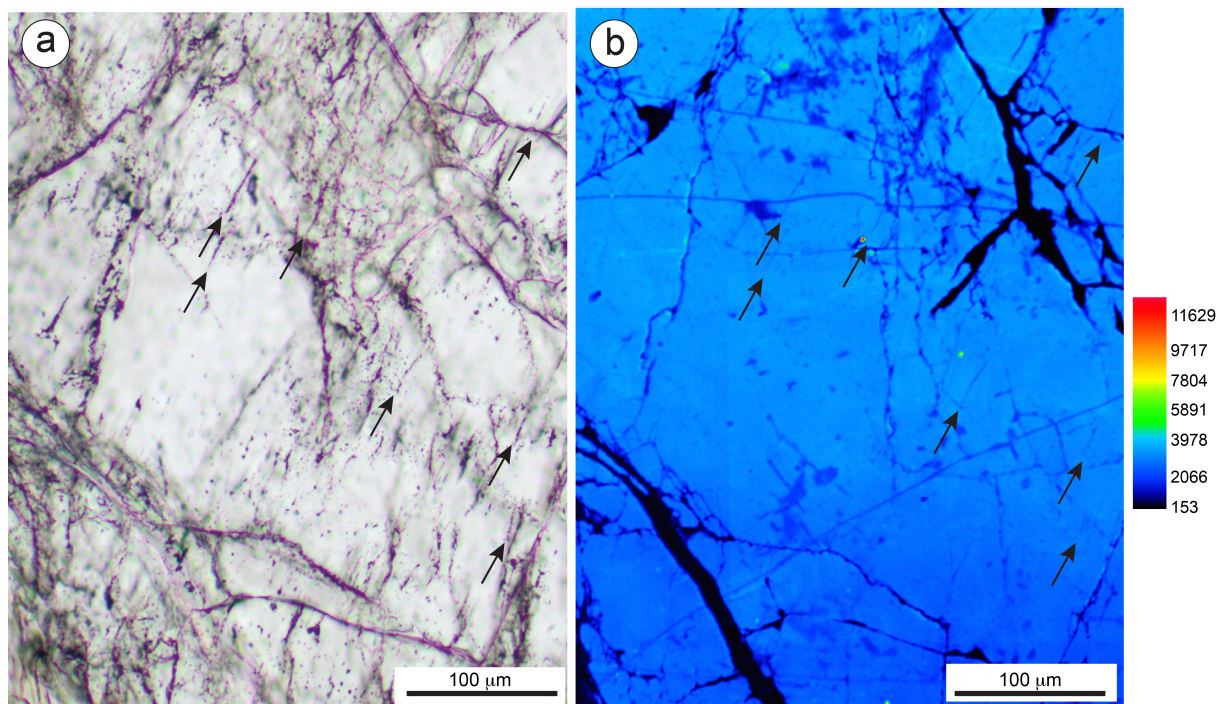


Figure S2 – Plane polarized microphotograph (a) and SEM-cathodoluminescence image (b) of the quartz studied by EBSD (Figure 4). The SEM-cathodoluminescence image was acquired on the Electron Probe X-ray Microanalyzer (EMPA) JEOL JX-8230 equipped with panchromatic cathodoluminescence system (ISTerre, Grenoble), with 15 kV acceleration voltage, 10 nA probe current, 1  $\mu\text{m}$  step size and 50 ms dwell time. Whereas the plane polarized micrograph integrates several tens  $\mu\text{m}$  in depth, cathodoluminescence image provides informations on the very near surface of the polished thin section. Therefore, microstructures visible on a may be not visible in b. The alignments of tiny fluid inclusions (black arrows) have a dark blue signature similar to quartz located near laumontite-filled microfractures suggesting both microstructures were healed by the same fluid. Note that some straight and thin microfractures (roughly E-W on the SEM cathodoluminescence image) have also the same dark blue signature but are not visible on the microphotograph in a) probably because they did not trapped fluid inclusions.

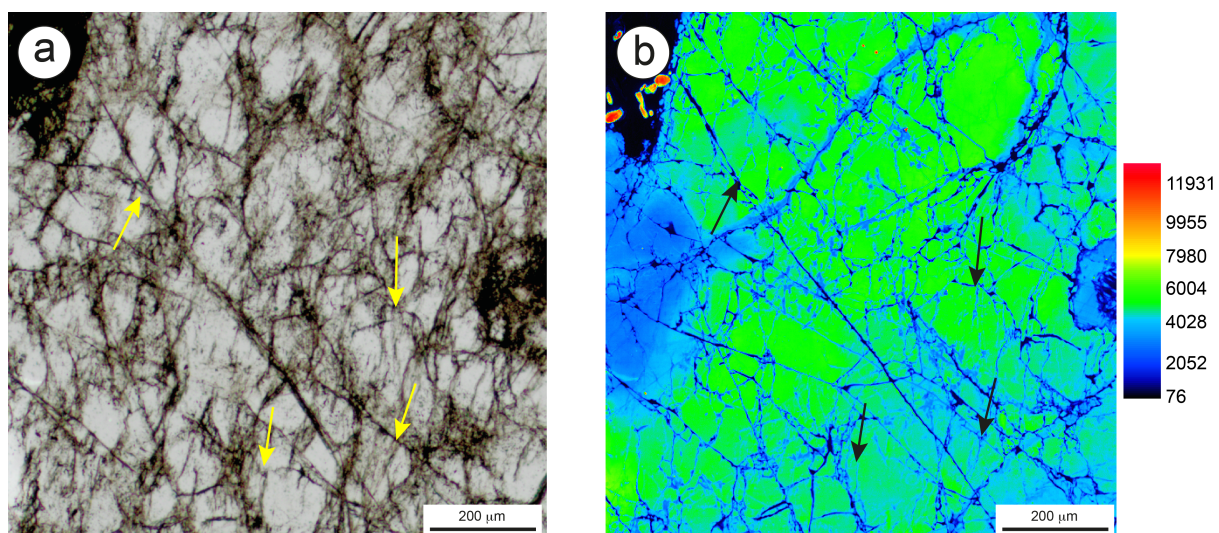


Figure S3 - Plane polarized microphotograph (a) and SEM-cathodoluminescence image (b) of the quartz studied by EBSD (Figure 7 and 8). The SEM-cathodoluminescence image was acquired on the Electron Probe X-ray Microanalyzer (EMPA) JEOL JX-8230 equipped with panchromatic cathodoluminescence system (ISTerre, Grenoble), with 15 kV acceleration voltage, 20 nA probe current, 1  $\mu\text{m}$  step size and 50 ms dwell time. Whereas the plane polarized micrograph integrates several tens  $\mu\text{m}$  in depth, cathodoluminescence image provides informations on the very near surface of the polished thin section. Therefore, microstructures visible on a may be not visible in b. The alignments of tiny fluid inclusions (yellow arrows on a, black arrows in b) have a dark blue signature similar to quartz located near laumontite-filled microfractures suggesting both microstructures were healed by the same fluid.

#### Supplementary Material 4: Mathematical transformations applied to the EBSD data in order to pass the orientation matrices and map points positions into the LaueTools sample reference frame

These transformations were used to generate figures 9 and 11b.

The x,y map positions in the LT "map" sample reference frame (given in figure 2a) were calculated using :

$$x\_map\_LT = x\_map\_EBSD$$

$$y\_map\_LT = -y\_map\_EBSD$$

A first orientation matrix  $t\_g\_matrix$  was calculated from the Bunge Euler angles (e.g. Bunge, 1982) of the Oxford Instruments \*.ctf file (components: 0 = Euler1, 1 = Euler2, 2 = Euler3), using the formula given by R. Quey at page 10 in the Orilib Manual

<https://sourceforge.net/projects/orilib/files/orilib/manual%201.1.1%20%28for%20orilib%201.1%29/orilib-man-1.1.1.pdf/download>

$$\phi_1 = \text{Euler3\_rad}[0]$$

$$\text{PHI} = \text{Euler3\_rad}[1]$$

$$\phi_2 = \text{Euler3\_rad}[2]$$

$$g_{11} = \cos(\phi_1) \cdot \cos(\phi_2) - \sin(\phi_1) \cdot \sin(\phi_2) \cdot \cos(\text{PHI})$$

$$g_{12} = \sin(\phi_1) \cdot \cos(\phi_2) + \cos(\phi_1) \cdot \sin(\phi_2) \cdot \cos(\text{PHI})$$

$$g_{13} = \sin(\phi_2) \cdot \sin(\text{PHI})$$

$$g_{21} = -\cos(\phi_1) \cdot \sin(\phi_2) - \sin(\phi_1) \cdot \cos(\phi_2) \cdot \cos(\text{PHI})$$

$$g_{22} = -\sin(\phi_1) \cdot \sin(\phi_2) + \cos(\phi_1) \cdot \cos(\phi_2) \cdot \cos(\text{PHI})$$

$$g_{23} = \cos(\phi_2) \cdot \sin(\text{PHI})$$

$$g_{31} = \sin(\phi_1) \cdot \sin(\text{PHI})$$

$$g_{32} = -\cos(\phi_1) \cdot \sin(\text{PHI})$$

$$g_{33} = \cos(\text{PHI})$$

$$g\_matrix = \text{array}([[g_{11}, g_{12}, g_{13}], [g_{21}, g_{22}, g_{23}], [g_{31}, g_{32}, g_{33}]])$$

$$t\_g\_matrix = g\_matrix.\text{transpose}()$$

Transformations were then applied to  $t\_g\_matrix$  using the criterion that for site 2, the final EBSD matrix should approximately match the microLaue matrix, following the three steps described below.

A first cartesian reciprocal unit cell (vectors  $a_0^*$ ,  $b_0^*$ ,  $c_0^*$ ) was created assuming that  $t\_g\_matrix$  gives the coordinates of  $-a_0^*$ ,  $-b_0^*$ ,  $c_0^*$  as columns on the x, y, z axes of the "orientation" EBSD sample reference frame (using the Matlab notation where  $\text{mat}[:,0]$  is the first column of the 3x3 mat matrix).

$$\text{Ustarsample}[:,0] = -t\_g\_matrix[:,0]$$

$$\text{Ustarsample}[:,1] = -t\_g\_matrix[:,1]$$

$$\text{Ustarsample}[:,2] = t\_g\_matrix[:,2]$$

Then a hexagonal reciprocal unit cell (vectors  $a^*$ ,  $b^*$ ,  $c^*$ ) (for describing the trigonal quartz unit cell)  $\text{matstarsample}_{3 \times 3}$  was built using :

$$\text{matstarsample}_{3 \times 3} = \text{dot}(\text{Ustarsample}, \text{Bstar})$$

where the reciprocal metric tensor  $\text{Bstar}$  describes the distorted shape of the reciprocal unit cell.

$\text{Bstar} =$

```
[[2.35029623e-01  1.17514812e-01 -2.97580061e-17]
[0.00000000e+00  2.03541624e-01 -1.13309289e-17]
[0.00000000e+00  0.00000000e+00  1.85048113e-01]]
```

This means that  $a_0^*$  is along  $a^*$  (direction + sense), *i.e.*  $a^*$  is the preferred direction for the orthonormalization process when building the reciprocal cartesian crystal frame from the reciprocal hexagonal unit cell.

A 180 degrees rotation of the matrix around the z-axis was then applied in order to obtain the coordinates of the reciprocal crystal vectors in the "orientation" microLaue sample reference frame described in figure 2a (rotated by 180 degrees around z with respect to the "orientation" EBSD sample reference frame).

matrot =

```
[[ -1.  -0.  0.]
[ 0.  -1.  0.]
[ 0.  0.  1.]]
```

matstarsample3x3\_rotated = dot(matrot, matstarsample3x3)

At this stage, due to the arbitrary way of naming the  $a^*$ ,  $b^*$ ,  $c^*$  reciprocal vectors when indexing, the matrix matstarsample3x3\_rotated recalculated from EBSD may still differ from the microLaue matrix by a rotation of 120 degrees around c and/or an inversion of c.

An "Euler angles minimization" process was therefore applied to get a single matrix for each crystallite.

From a given set of ( $a^*$ ,  $b^*$ ,  $c^*$ ) vectors, 6 equivalent matrices ( $a^*_new$ ,  $b^*_new$ ,  $c^*_new$ ) can be built :

( $a^*$ ,  $b^*$ ,  $c^*$ ), ( $-a^*+b^*$ ,  $-a^*$ ,  $c^*$ ), ( $-b^*$ ,  $a^*-b^*$ ,  $c^*$ ) (120 degrees rotations around c)

( $b^*$ ,  $a^*$ ,  $-c^*$ ), ( $a^*-b^*$ ,  $-b^*$ ,  $-c^*$ ), ( $-a^*$ ,  $b^*-a^*$ ,  $-c^*$ ) (180 degrees rotation around  $a^*+b^*$  then 120 degrees rotations around c)

The criteria used to choose between these 6 matrices was the following :

- the z-coordinate of  $c^*_new$  should be positive (choice between  $+c^*$  and  $-c^*$ )

- the x-coordinate of  $a^*_new$  should be maximal (choice between the three matrices with the same  $c^*_new$ )

This minimization process is important to ensure that all the map points belonging to closely oriented crystallites end up with similar matrices: this allows plotting usable histograms of orientation matrix components, and using these histograms to define thresholds on the orientation matrix components to class the map points according to the crystallite they belong to, and calculate the average orientation matrix of a given crystallite.

Reference:

Bunge, H.-J.: Texture analysis in materials science – Mathematical methods, Butterworths, London, UK, 1982.

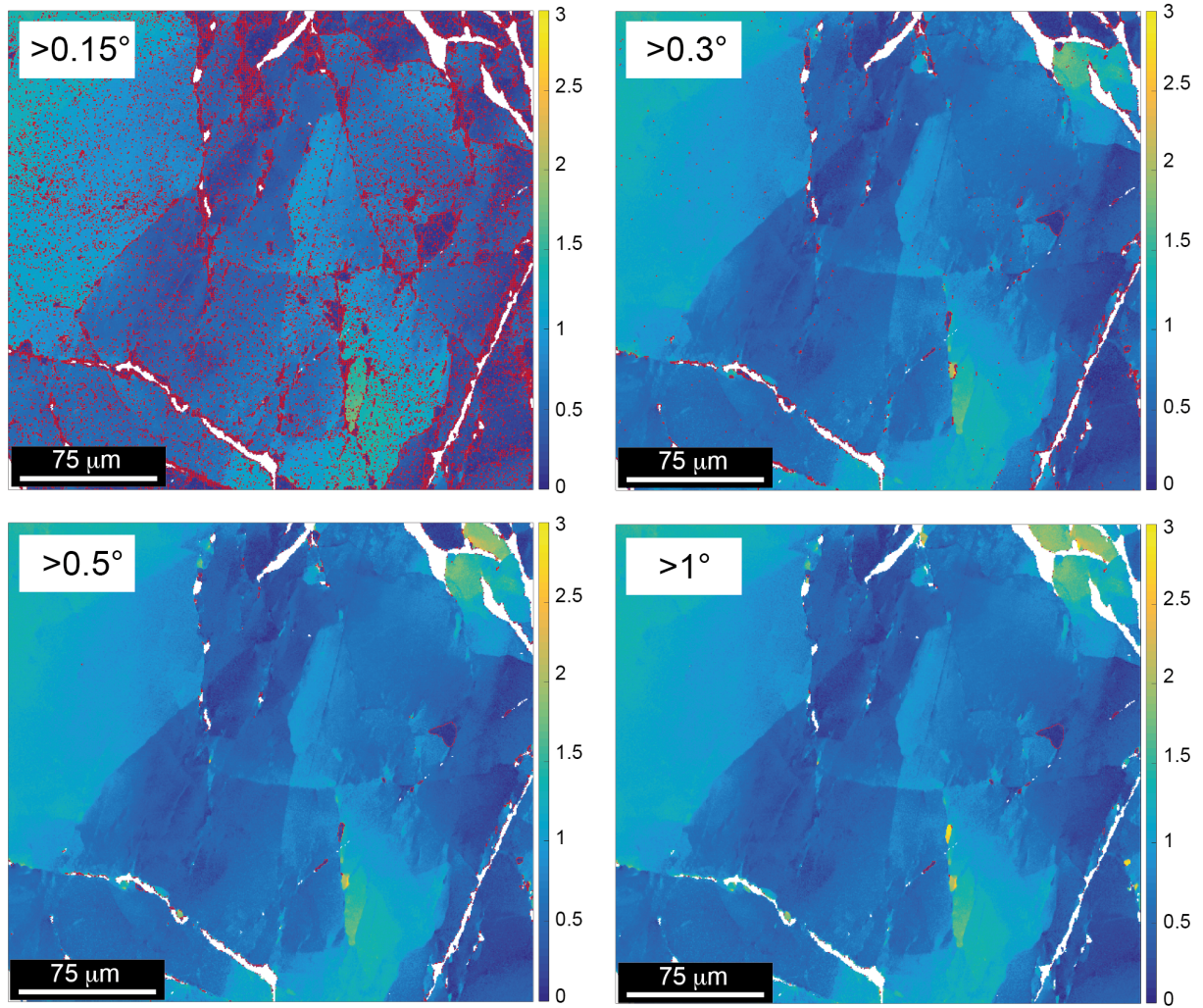


Figure S5 – Misorientation domains in the area studied in detail (Figure 10). The vertical or horizontal limits between pixels showing a misorientation greater than  $0.15^\circ$  (a),  $0.3^\circ$  (b),  $0.5^\circ$  (c) and  $1^\circ$  (d) are coloured in red.

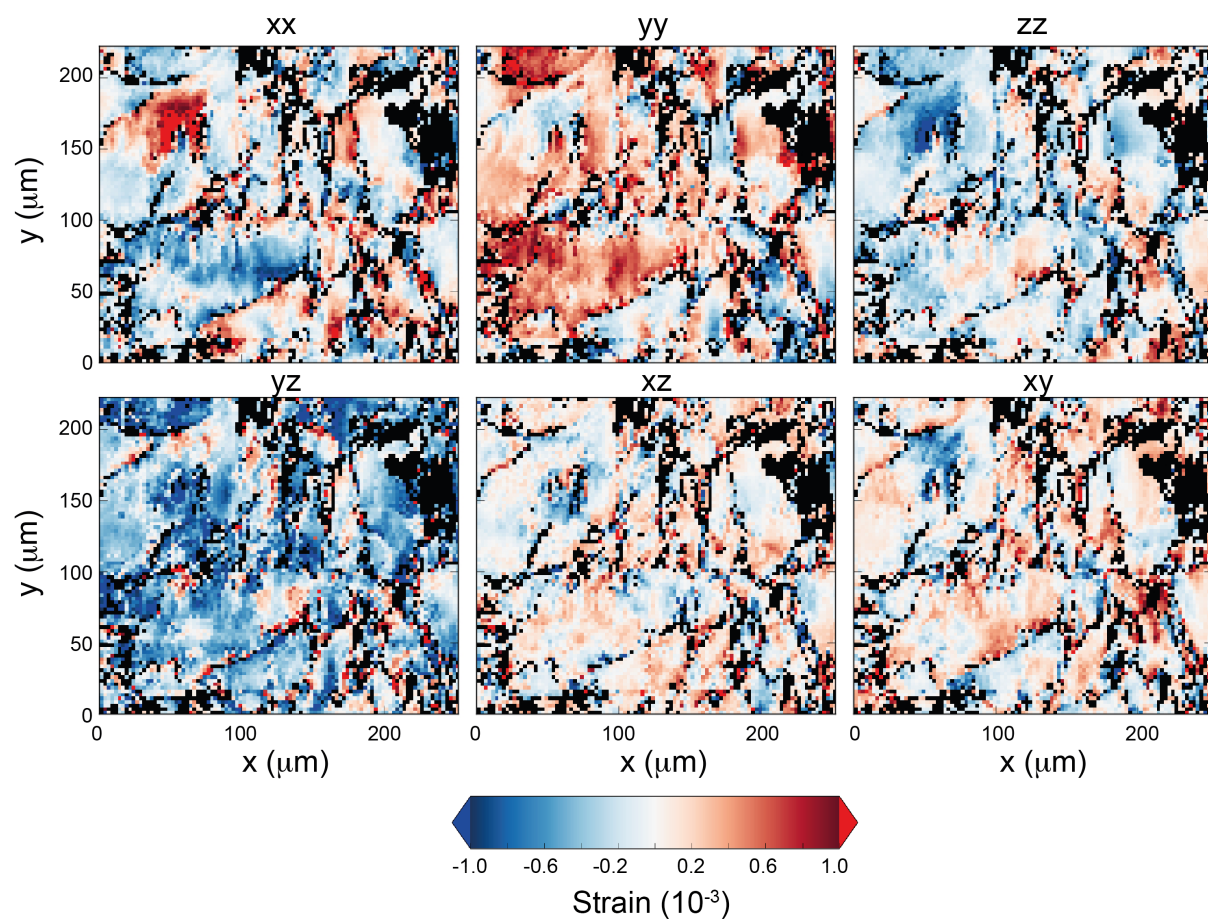


Figure S6 - Laue microdiffraction : maps of the six components of the deviatoric strain tensor, in the sample reference frame. Black points were filtered out based on the criteria described in Figure A3d.